Robustness Analysis of a Synthetic Translational Resource Allocation Controller

Alexander P. S. Darlington, Jongrae Kim, and Declan G. Bates

***Abstract*—Recent research in synthetic biology has highlighted the potential of translational resource allocation controllers to improve circuit modularity by dynamically allocating finite cellular resources in response to fluctuating circuit demands. The design of such controllers is complicated by the significant levels of parametric uncertainty that arise in their biological implementations. Tools from robust control, such as μ-analysis, can be used to determine the robustness of controller designs to parametric uncertainty, but require further development to allow their application to biomolecular control systems, which are typically highly non-linear, and contain multiple uncertainties that cannot be represented using the standard linear fractional transformation formalism. Here, we show how an linear fractional transformation-free formulation of the μ-analysis problem can be used to analyze and compare the robustness of alternative potential implementations of a translational resource allocation controller that utilises orthogonal "circuit-specific" ribosomes to translate circuit genes. Our results provide useful guidelines for the construction of robust resource allocation circuitry for multiple future biotechnological applications.**

***Index Terms*—**

I. Introduction

SYNTHETIC circuits can be created to perform complex computations and information processing within cells by assembling genetic modules. During the circuit design process it is typically assumed that each module is independent (bar the designed interactions), however, it is now well established that additional unexpected interactions may emerge as a consequence of the sharing of cellular resources [1]. This breakdown in modularity may not be apparent from gene network models or circuit diagrams during the design phase, and can subsequently lead to loss of functionality or even circuit failure upon implementation in host organisms.

The sharing of translational resources, in the form of free ribosomes, has been implicated as a crucial cause of these non-regulatory interactions [2], [3], since during exponential growth, the pool of ribosomes needed for translation of mRNA (messenger Ribonucleic Acid) into protein is constant [4], and this finite pool of ribosomes is shared across all genes requiring translation. Although similar limitations exist at the transcriptional level, in many settings the resulting effects are small and hence can be neglected [3].

To address the above problems, a prototype translational allocation controller was recently designed and successfully implemented experimentally [5]. This controller utilises orthogonal 'circuit-specific' ribosomes which exclusively translate circuit genes. By dynamically controlling the production of such orthogonal ribosomes, the effects of resource limitations on the gene circuit can be reduced, as circuit-specific translational capacity is increased as demand increases. These o-ribosomes are created by expressing a synthetic rRNA (ribosomal RNA)-based component which displaces a core host ribosomal component, changing the machinery's specificity from host genes to circuit genes [6].

The resource allocation controller regulates the production of this synthetic ribosomal component using negative feedback, as shown in Figure 1. The size of the circuit-specific o-ribosome pool is controlled by the use of a repressive transcription factor protein. The protein acts to inhibit the production of the synthetic ribosomal component by sequestering the latter's promoter (and so preventing RNA polymerase binding and transcription). The protein is constitutively expressed and translated by the circuit-specific pool. It therefore acts as a sensor of translational demand; as demand increases, the level of this protein falls and *vice versa*. The inhibitory action of the protein acts to invert this demand signal as it is relayed to the synthetic ribosomal RNA promoter; as protein concentration falls, repression of the promoter through sequestration by the controller protein falls and hence rRNA synthesis increases (and *vice versa*). Therefore co-option of ribosomes from the host to the circuit-specific pool follows the fluctuating demands made by the circuit.

In [7], we developed a mathematical model of the translational resource allocation controller shown in Figure 1. Due to the underlying biological mechanisms, this model contains many non-linear terms, and as shown below, consideration of uncertainty arising in biological implementations leads to a

Manuscript received May 30, 2018; revised August 7, 2018; accepted August 21, 2018. Date of publication August 28, 2018; date of current version November 6, 2018. This work was supported in part by the University of Warwick, in part by EPSRC and BBRSRC Centre for Doctoral Training in Synthetic Biology under Grant EP/L016494/1, and in part by the Leverhulme Trust under Grant RPG-2017-284. Recommended by Senior Editor F. Blanchini. *(Corresponding author: Declan G. Bates.)*

A. P. S. Darlington and D. G. Bates are with the Warwick Integrative Synthetic Biology Centre, School of Engineering, University of Warwick, Coventry CV4 7AL, U.K. (e-mail: a.p.s.darlington@warwick.ac.uk; d.g.bates@warwick.ac.uk).

J. Kim is with the Institute of Design, Robotics and Optimisation, School of Mechanical Engineering, University of Leeds, Leeds LS2 9JT, U.K. (e-mail: menjkim@leeds.ac.uk).

This paper has supplementary downloadable material available at http://ieeexplore.ieee.org, provided by the author.

Digital Object Identifier 10.1109/LCSYS.2018.2867368

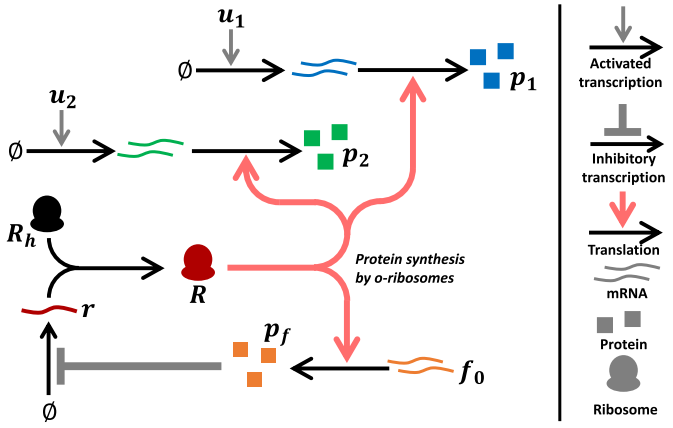

Fig. 1. Genetic architecture of the translational controller. Transcription of the mRNA for proteins p_1 and p_2 is activated by the inputs u_1 and u_2 respectively. p_f inhibits the transcription of the synthetic ribosomal RNA r. The synthetic RNA converts host-specific ribosomes R_h into circuit-specific ribosomes R which translate all circuit mRNAs and the mRNA of the controller gene into proteins.

closed-loop system containing large numbers of real uncertainties (typically kinetic rate constants) that do not enter the linearised system dynamics as polynomial fractions. This poses significant challenges for the application of robustness analysis methods such as μ-analysis, which typically requires the uncertain system to be represented as a linear fractional transformation (LFT), and therefore no formal analysis of the controller's robustness was attempted in [7].

To address this issue, we here further develop an approach, first proposed in [9] and [10], based on combining a randomisation algorithm with a geometric interpretation of the μ-analysis problem. In this approach, the uncertainty is redefined by a subtraction between the uncertain system and the nominal system. Thus the procedure does not require that the uncertain parameters are actually decoupled from the system (as with LFTs) but only requires the evaluation of the difference between the nominal system and the perturbed system.

II. Modelling Uncertainty in a Translational Resource Allocation Control System

Here, we describe the non-linear closed-loop system model, derive its linearisation, and consider the way in which uncertain parameters affect the system. Definitions and nominal values for all parameters in the model are shown in Table I. The non-linear model describes the dynamics of a simple two gene circuit encoding proteins (species p_1 and p_2) and the controller system (species p_f, r and R_h). The controller consists of the synthetic rRNA species (r), the host ribosomes (R_h) and the protein p_f which controls the rate of rRNA synthesis. R represents the free orthogonal ribosome pool.

The dynamics of each circuit protein (p_i) follow:

$$\dot{p}_i = \gamma_i R \hat{c}_i - d_{p_i} p_i \tag{1}$$

where $\dot{p}_i$ is the derivative of p_i with respect to time and

$$\hat{c}_i = \frac{1}{k_{L_i}} \frac{n_R \tau_i}{d_{m_i}} \left(\frac{\sigma_T \hat{x}_i}{1+\hat{x}_i} \right), \quad \hat{x}_i = \frac{n_\sigma g_{i,T}}{k_{X_i}} \left(\frac{{u_i}^{\eta_i}}{{u_i}^{\eta_i} + \mu_i} \right) \tag{2}$$

TABLE I
Circuit and Controller Parameters

	Description	Nominal	Units
n_σ	Number of RNAP per gene	10	
σ_T	RNAP concentration	250	nM
n_R	Number of Ribosomes per mRNA	20	
R_T	Total ribosome concentration	2500	nM
η_i	Co-operativity of the input	1	
μ_i	Threshold of the input	10	nM
$g_{i,T}$	Gene i copy number	10	nM
k_{X_i}	Gene i promoter RNAP dissociation constant	200	nM
τ_i	Gene i mRNA synthesis rate	320	h^{-1}
k_{L_i}	Gene i mRNA-ribosome dissociation constant	10^5	nM
γ_i	p_i translation rate	240	h^{-1}
d_{m_i}	Gene i mRNA decay rate	20	h^{-1}
d_{p_i}	Gene i protein decay rate	1	h^{-1}
$g_{r,T}$	Synthetic rRNA copy number	500	nM
k_{X_r}	rRNA P_{lac} (P_{tet}) promoter dissociation constant	500 (350)	nM
τ_r	rRNA transcription rate	190	h^{-1}
d_r	rRNA decay rate	20	h^{-1}
ϱ_f	r:R_h association rate	0.9	$(nM \cdot h)^{-1}$
ϱ_r	R dissociation rate	24.8	h^{-1}
$g_{f,T}$	p_f copy number	10	nM
k_{X_f}	p_f promoter RNAP dissociation constant	500	nM
τ_f	Gene f transcription rate	320	h^{-1}
k_{L_f}	Gene f mRNA-ribosome dissociation constant	10^5	nM
γ_f	p_f translation rate	240	h^{-1}
d_{m_f}	Gene f mRNA decay rate	20	h^{-1}
d_{p_f}	p_f decay rate	1	h^{-1}
η_f	$lacI$ ($tetR$) co-operativity	4 (2)	
μ_f	$lacI$ ($tetR$) dissociation constant	0.02 (5.6)	nM

The dynamics of the protein controlling synthetic rRNA synthesis is given by:

$$\begin{aligned}\dot{p}_f = {} & \gamma_f R \hat{c}_f - d_{p_f} p_f \\ & - \eta_f (n_\sigma g_{r,T} - x_r - \kappa_r) {p_f}^{\eta_f} + \eta_f \mu_f \kappa_r \end{aligned} \tag{3}$$

where

$$\hat{c}_f = \frac{1}{k_{L_f}} \frac{n_R \tau_f}{d_{m_f}} \left(\frac{\sigma_T \hat{x}_f}{1+\hat{x}_f} \right) \quad \text{and} \quad \hat{x}_f = \frac{n_\sigma g_{f,T}}{k_{X_f}} \tag{4}$$

The inhibitory action of p_f at the rRNA promoter is given by

$$x_r = (\hat{x}_r \sigma_T)/(1+\hat{x}_r) \tag{5}$$

$$\hat{x}_r = (n_\sigma g_{r,T}/k_{X_r})/[\mu_f/(\mu_f + {p_f}^{\eta_f})] \tag{6}$$

$$\kappa_r = (n_\sigma g_{r,T} - x_r)[{p_f}^{\eta_f}/({p_f}^{\eta_f} + \mu_f)] \tag{7}$$

The dynamics of the synthetic rRNA are given by:

$$\dot{r} = \tau_r x_r - d_r r - \varrho_f r R_h + \varrho_r R \tag{8}$$

(Note the action of p_f through x_r). The dynamics of the host ribosome pool are given by:

$$\dot{R}_h = -\varrho_f r R_h + \varrho_r R \tag{9}$$

As the number of ribosomes is fixed, the total number of orthogonal ribosomes ($R_{o,T}$) is given by $R_T - R_h$ (total ribosomes minus the host ribosomes). These are distributed across all protein encoding circuit and controller genes such that the number of free orthogonal ribosomes is:

$$R = \frac{R_T - R_h}{1 + \hat{c}_f + \Sigma_1^N (\hat{c}_i)} \tag{10}$$

The non-linear model is formed by (1) (repeated once for each circuit gene i, here we consider two circuit genes) and (3) to (9). We can define the vector $\mathbf{y} := [p_1,\ p_2,\ p_f,\ r,\ R_h]^T$. We define $\bar{\mathbf{y}}$ to be the solution to $\dot{\mathbf{y}} = \mathbf{0}$ and linearise the system around this point.

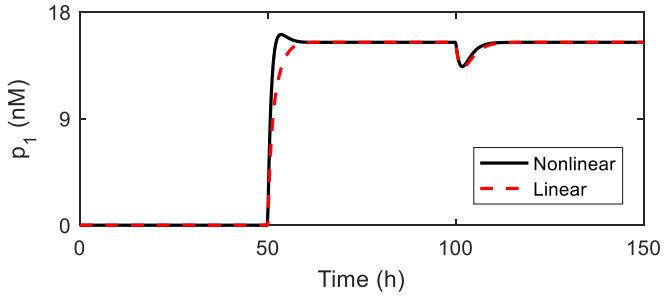

Fig. 2. Simulations of the non-linear closed-loop system and its linearisation for the *lacI*-based Controller 1. Only p_1 is shown. Parameters are listed in Table I. Inputs: $u_1 = u_2 = 0$ nM while $t < 50$ h. From $t > 50$ h, $u_1 = 500$ nM. From $t > 100$ h, $u_2 = 500$ nM.

The linearisation is $\dot{\mathbf{x}} = A|_{y=\bar{y}}\mathbf{x}$ where $\mathbf{x} = \mathbf{y} - \bar{\mathbf{y}}$ and A is the Jacobian. The Jacobian of the system is:

$$A = \begin{bmatrix} -d_{p_1} & 0 & 0 & 0 & -(\gamma_1\hat{c}_1)/K_1 \\ 0 & -d_{p_2} & 0 & 0 & -(\gamma_2\hat{c}_2)/K_1 \\ 0 & 0 & -d_{p_f} & 0 & -(\gamma_f\hat{c}_f)/K_1 \\ 0 & 0 & -K_2 & -d_r - \varrho_f\bar{R}_h & -\varrho_f\bar{r} - \varrho_r/K_1 \\ 0 & 0 & 0 & -\varrho_f\bar{R}_h & -\varrho_f\bar{r} - \varrho_r/K_1 \end{bmatrix} \tag{11}$$

where K_1 and K_2 expand to:

$$K_1 = 1 + \hat{c}_f + \hat{c}_1 + \hat{c}_2 \tag{12}$$

$$K_2 = \frac{\sigma_T\eta_f n_\sigma g_{r,T} k_{X_f}\mu_f \bar{p}_f^{\eta_f}\tau_f}{\bar{p}_f(n_\sigma g_{r,T}\mu_f + k_{X_f}\mu_f + k_{X_f}\bar{p}_f^{\eta_f})^2} \tag{13}$$

Figure 2 shows simulations confirming good agreement between the linear and non-linear models for a biological implementation based on the lacI repressor. Upon induction of p_2 at 100 h, the translational resource allocation controller successfully rejects the disturbance to p_1 caused by resource mediated coupling.

In general, the Jacobian, A, includes m uncertain parameters, δ, which is an element of $\mathbb{R}^m$, i.e., $A = A(\delta)$. All δ can be decoupled from the nominal system, if all the δ in the elements of A appear as polynomial fractions, and the resulting LFT is given by:

$$\dot{\mathbf{x}} = A(0)\mathbf{x} + B\mathbf{w} \tag{14}$$

$$\mathbf{z} = C\mathbf{x} + D\mathbf{w} \tag{15}$$

$$\mathbf{w} = \Delta\mathbf{z} \tag{16}$$

where $A(0)$ is the nominal system and stable, and Δ is a diagonal matrix of the uncertain parameters δ. If a system can be represented in this form then the μ-analysis problem becomes a search for the minimum magnitude δ which gives:

$$|I - M(j\omega)\Delta| = 0 \tag{17}$$

where $|\cdot|$ is the determinant, $j = \sqrt{-1}$, $\omega = [0, \infty)$ and $M(j\omega) = [j\omega I - A(0)]^{-1}$ and I is the identity matrix whose dimension is the same as A. Computationally efficient algorithms exist to find μ-bounds for these systems.

Parametric uncertainty arises in synthetic circuits due to (i) noise in the original measurement (e.g., due to population effects), (ii) changes in transcription/translational kinetics due to new DNA context for genetic 'parts' (e.g., [8]) and (iii) fluctuations due to growth conditions/stains (e.g., [2]).

In our model we consider all non-input parameters (i.e., all except u_1 and u_2) to be uncertain, and model the variability of a given parameter κ as $(1 + \delta)\kappa$ where κ is the nominal value and δ is the perturbation. Re-considering the linearised model with these added uncertainties shows that it cannot be represented in the necessary form depicted in (14)-(16), as the δ are not polynomial fractions, nor can the uncertain parameters be presented as a diagonal matrix Δ. This is apparent by inspection of the Jacobian in (11), substituting the disturbances δ_x (where x represents the index of the value in the uncertainty vector δ) yields:

$$\begin{bmatrix} -(1+\delta_{12})d_{p_1} & 0 & 0 & \vdots & \vdots \\ 0 & -(1+\delta_{21})d_{p_2} & 0 & \vdots & \vdots \\ 0 & 0 & -(1+\delta_{34})d_{p_f} & M_1 & M_2 \\ 0 & 0 & -K_2(\delta) & \vdots & \vdots \\ 0 & 0 & 0 & \vdots & \vdots \end{bmatrix} \tag{18}$$

where M_1 and M_2 are the fourth and fifth columns of the uncertain Jacobian:

$$M_1 = \begin{bmatrix} 0 \\ 0 \\ 0 \\ -(1+\delta_{25})d_r - (1+\delta_{26})\varrho_f\bar{R}_h(\delta) \\ -(1+\delta_{26})\varrho_f\bar{R}_h(\delta) \end{bmatrix} \tag{19}$$

$$M_2 = \begin{bmatrix} -[(1+\delta_{10})\gamma_1\hat{c}_1(\delta)]/K_1(\delta) \\ -[(1+\delta_{19})\gamma_2\hat{c}_2(\delta)]/K_1(\delta) \\ -[(1+\delta_{32})\gamma_f\hat{c}_f(\delta)]/K_1(\delta) \\ -(1+\delta_{26})\varrho_f\bar{r}(\delta) - [(1+\delta_{27})\varrho_r]/K_1(\delta) \\ -(1+\delta_{26})\varrho_f\bar{r} - [(1+\delta_{27})\varrho_r]/K_1(\delta) \end{bmatrix} \tag{20}$$

$K_1(\delta)$ and $K_2(\delta)$ take the same form as in (13) but with added perturbations:

$$K_1 = 1 + \hat{c}_f(\delta) + \hat{c}_1(\delta) + \hat{c}_2(\delta) \tag{21}$$

$$K_2 = \frac{K_{2,1}K_{2,2}\bar{p}_f(\delta)^{(1+\delta_{37})\eta_f}}{\bar{p}_f(\delta)[K_{2,3} + K_{2,4} + (1+\delta_{29})k_{X_f}\bar{p}_f(\delta)^{(1+\delta_{37})\eta_f}]^2} \tag{22}$$

where

$$\hat{c}_f(\delta) = \frac{1}{(1+\delta_{31})k_{L_f}} \frac{(1+\delta_4)n_R(1+\delta_{30})\tau_f}{(1+\delta_{33})d_{m_f}} \frac{(1+\delta_1)\sigma_T\hat{x}_f(\delta)}{1+\hat{x}_f(\delta)} \tag{23}$$

$$\hat{x}_f(\delta) = [(1+\delta_3)n_\sigma(1+\delta_{35})g_{f,T}]/((1+\delta_{29})k_{X_f}) \tag{24}$$

$$\hat{c}_1(\delta) = \frac{1}{(1+\delta_9)k_{L_1}} \frac{(1+\delta_4)n_R(1+\delta_8)\tau_1}{(1+\delta_{11})d_{m_1}} \frac{(1+\delta_1)\sigma_T\hat{x}_1(\delta)}{1+\hat{x}_1(\delta)} \tag{25}$$

$$\hat{x}_1(\delta) = \frac{(1+\delta_3)n_\sigma(1+\delta_{13})g_{1,T}}{(1+\delta_7)k_{X_1}} \frac{u_1^{(1+\delta_5)\eta_1}}{u_1^{(1+\delta_5)\eta_1} + (1+\delta_6)\mu_1} \tag{26}$$

$$\hat{c}_2(\delta) = \frac{1}{(1+\delta_{18})k_{L_2}} \frac{(1+\delta_4)n_R(1+\delta_{17})\tau_2}{(1+\delta_{20})d_{m_2}} \frac{(1+\delta_1)\sigma_T\hat{x}_2(\delta)}{1+\hat{x}_2(\delta)} \tag{27}$$

$$\hat{x}_2(\delta) = \frac{(1+\delta_3)n_\sigma(1+\delta_{22})g_{2,T}}{(1+\delta_{16})k_{X_2}} \frac{u_2^{(1+\delta_{14})\eta_2}}{u_2^{(1+\delta_{14})\eta_2} + (1+\delta_{15})\mu_2} \tag{28}$$

$$K_{2,1} = (1+\delta_1)\sigma_T(1+\delta_{37})\eta_f(1+\delta_3)n_\sigma(1+\delta_{28})g_{r,T} \tag{29}$$

$$K_{2,2} = (1+\delta_{29})k_{X_f}(1+\delta_{36})\mu_f(1+\delta_{30})\tau_f \tag{30}$$

$$K_{2,3} = (1+\delta_3)n_\sigma(1+\delta_{28})g_{r,T}(1+\delta_{36})\mu_f \tag{31}$$

$$K_{2,4} = (1+\delta_{29})k_{X_f}(1+\delta_{36})\mu_f \tag{32}$$

We also reformulate the steady states of the species $\bar{\mathbf{y}}$ with the uncertainties (e.g., $\bar{r}(\delta)$ is the value of $\bar{r}$ including the necessary perturbations from the δ vector).

Since the 36 independent uncertain parameters affecting this closed-loop system cannot be represented in the standard LFT-based form required for μ-analysis, in the following we describe an alternative 'LFT-free' approach, that will allow us to rigorously quantify the robustness of this controller (see also the Supplementary Material for a tutorial example).

III. LFT-Free μ-Analysis

To implement the LFT-free method we first consider a new representation for the uncertainties:

$$A_\Delta(\delta) \coloneqq A(\delta) - A(0) \tag{33}$$

The original uncertain LTI system can be now expressed as

$$\dot{\mathbf{x}} = A(0)\mathbf{x} + A_\Delta(\delta)\mathbf{x} \tag{34}$$

Taking the Laplace transform gives:

$$X(s) = M(s)A_\Delta(\delta)X(s) + M(s)\mathbf{x}(0) \tag{35}$$

where $X(s)$ is the Laplace transform $\mathbf{x}(t)$, $M(s) = [sI - A(0)]^{-1}$, and $\mathbf{x}(0)$ is the initial condition of $\mathbf{x}(t)$.

The robustness problem may be formulated as a search for the δ of smallest magnitude which satisfies:

$$|I - M(j\omega)A_\Delta(\delta)| = 0 \tag{36}$$

for all frequencies $\omega \in [0, \infty)$. We can now formulate the μ-analysis problem as follows.

Find the $\underline{\mu}$ (lower bound) and $\bar{\mu}$ (upper bound) such that $\underline{\mu} \leq \mu(\omega) \leq \bar{\mu}$, for $\omega \in [0, \infty)$, where

$$\mu(\omega) = \begin{cases} 0, & |I - M(j\omega)A_\Delta(\delta)| \neq 0 \text{ for all } \delta, \\ [d_{\min}(\omega)]^{-1}, & \text{otherwise}, \end{cases} \tag{37}$$

where

$$d_{\min}(\omega) = \min\{d \mid \exists \delta \in \mathbb{R}^m, \text{ such that } |I - M(j\omega)A_\Delta(\delta)| = 0\}$$

The uncertainty in this problem has no general analytical expression and so standard μ-bound estimation algorithms cannot be applied. However, we can obtain the value for a specific δ by evaluating (33). The singularity condition of the determinant is then given by:

$$\begin{aligned} f_R(\delta) &= \Re|I - M(j\omega)A_\Delta(\delta)| = 0 \\ f_I(\delta) &= \Im|I - M(j\omega)A_\Delta(\delta)| = 0 \end{aligned} \tag{38}$$

where $\Re(\cdot)$ and $\Im(\cdot)$ denote the real and imaginary parts of a complex number, [9], [10]. These two equalities are $(m-1)$-dimensional manifolds on the m-dimensional uncertainty space δ. The manifolds divide the uncertainty space into four sections (Figure 3). The exact value of μ is the inverse of the norm of the δ where the two manifolds meet at the singular point (the point highlighted in Figure 3). Any norm could be used in general and the infinity-norm is a frequent choice in μ-analysis.

Note firstly that, for $A_\Delta(0) = 0$, i.e., the nominal system, $I - M(j\omega)A_\Delta(\delta)$ is equal to the identity matrix and the determinant is 1. The real part is 1 and the imaginary part is 0 at $\delta = 0$. Therefore, under the assumption of nominal stability, the manifold where the imaginary part is equal to zero always passes through the origin in the uncertain space, whereas the other manifold, where the real part is equal to zero, always stays away from the origin with a strictly positive distance as depicted in Figure 3. Secondly, the uncertainty space can be divided into four sections:

$$\begin{aligned} s_1 &= \{\delta \mid f_R(\delta) > 0 \text{ and } f_I(\delta) > 0\} \\ s_2 &= \{\delta \mid f_R(\delta) > 0 \text{ and } f_I(\delta) < 0\} \\ s_3 &= \{\delta \mid f_R(\delta) < 0 \text{ and } f_I(\delta) < 0\} \\ s_4 &= \{\delta \mid f_R(\delta) > 0 \text{ and } f_I(\delta) < 0\} \end{aligned} \tag{39}$$

with each section shown in Figure 3. Now, the number of sign combinations found on boundary boxes of different sizes in the uncertainty space can be counted. In Figure 4, for example, the number of sign combinations on boxes $\mathbf{B}_1$ and $\mathbf{B}_2$ are three and four, respectively. Once four sign combinations are found, it can be concluded that the value of μ is inside that box (here box $\mathbf{B}_2$). This leads to the following

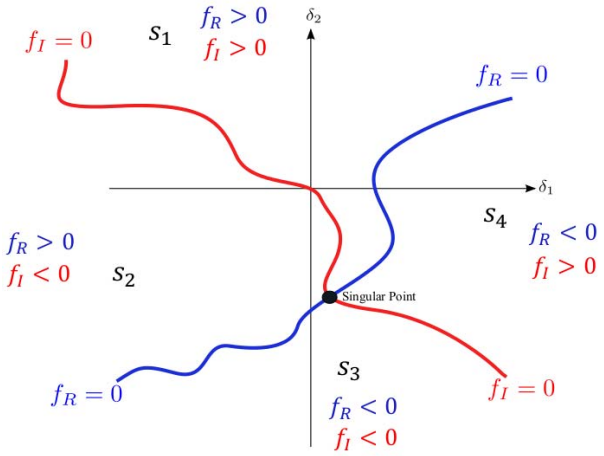

Fig. 3. Interaction of two surfaces and the four possible sign combinations, s_i for $i = 1,\ 2,\ 3$ and 4, in $m = 2$ uncertain space.

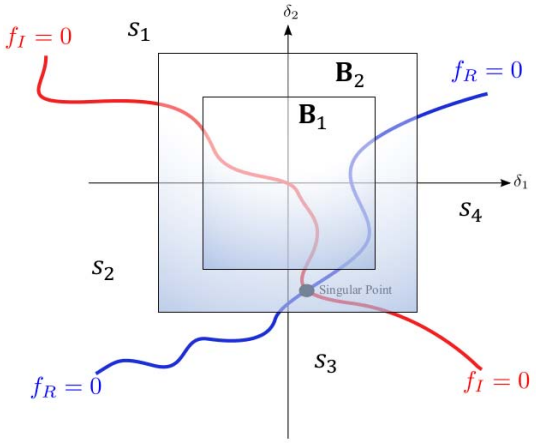

Fig. 4. The number of sign combinations found along the edges of $\mathbf{B}_1$ is three and thus the size of the box provides a μ-upper bound. On the other hand, the number of sign combinations found along the edges of $\mathbf{B}_2$ is four and thus the size of this box provides a μ-lower bound.

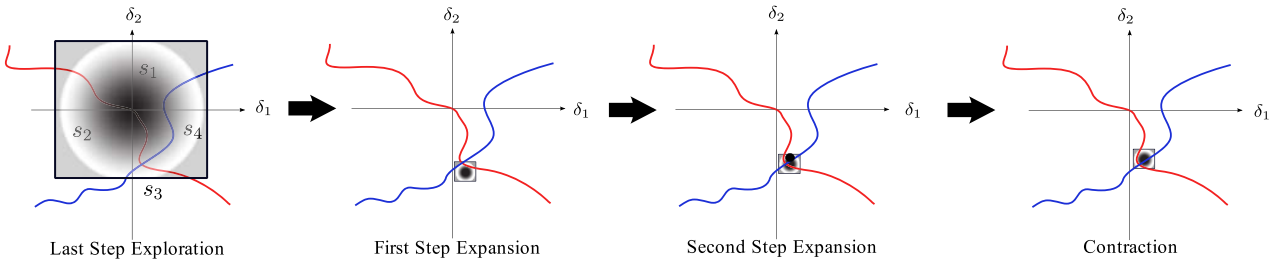

Fig. 5. μ-lower bound expansion and contraction steps.

algorithms for finding upper and lower bounds on μ (see the Supplementary Material for formal proofs of convergence for these algorithms and MATLAB code for a numerical example).

A. μ-Upper Bound Algorithm

1. Check the sign of the real and imaginary parts of the determinant, $I - MA_\Delta$, for uniform random samples δ inside a hyperbox centred at the origin in the uncertain space, e.g., $\mathbf{B}_1$ or $\mathbf{B}_2$ in Figure 4, until either the maximum number of samples is reached or all four sign combinations are found.

2. If the combinations are not found, increase the size of the hyperbox, otherwise decrease the size of the hyperbox, and repeat. The inverse of the maximum box size which includes samples containing only three sign combinations is the upper bound, e.g., s_1, s_2 and s_4 in $\mathbf{B}_1$ in Figure 4.

This algorithm is less conservative than the original algorithm presented in [10] as it allows three rather than two sign combinations, as shown in Figure 4.

B. μ-Lower Bound Algorithm

1. *Exploration:* Check the sign of the real and imaginary parts of the determinant, $I - MA_\Delta$, for uniform random samples δ on the faces of a hyperbox centred at the origin in the uncertain space, until either the maximum number of samples is reached or the four sign combinations are found. If the combinations are not found, increase the size of the hyperbox.

2. *Expansion & Contraction:* In Figure 4 the last sign combination found in $\mathbf{B}_2$ from the *Exploration* step is most likely to be s_3 as this is the smallest area compared to the others. Checking the sign combinations of random samples inside the box, whose centre is δ corresponds to the sign combination found last in the *Exploration* step. The initial box size is the maximum tolerance value. If all sign combinations are not found by the maximum sampling number, the box size is increased. If all sign combinations are found, but the size of the box is greater than the tolerance, move the centre of the box to δ, which is in the middle between two δ's whose sign combinations were found last and second last. Repeat these steps until some pre-defined maximum number of iterations is reached (in which case the lower bound is zero), or all sign combinations are found in a box centred close to the singular point, where the box size is equal to the given tolerance (in which case the lower bound is the inverse of the distance from the singular point to the origin). A graphical illustration of the procedure is given in Figure 5.

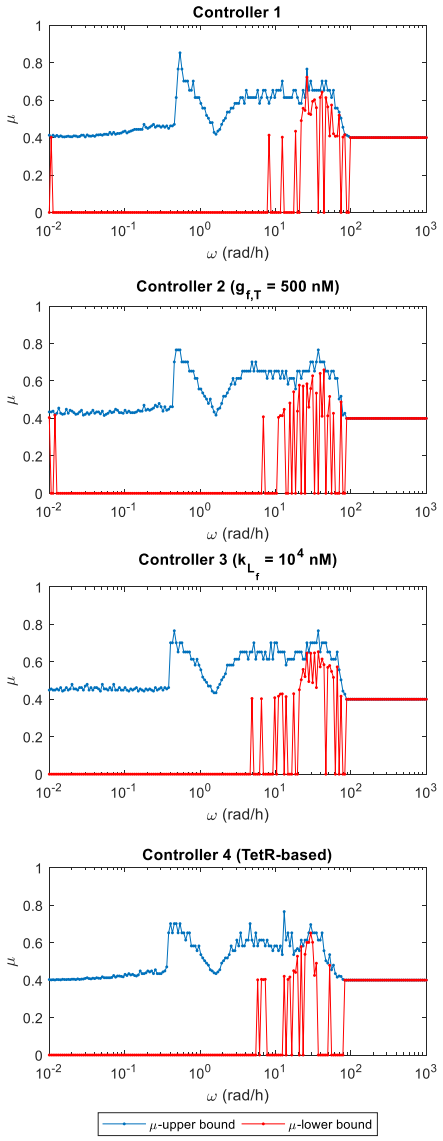

Fig. 6. μ-lower and upper bounds for different potential biological implementations scaled by $\pm$ 40%. Controller 1 corresponds to the *lacI*-based design whose parameters are listed in Table I. Controller 2 corresponds to an increase in gene copy number to $g_{f,T} = 500$ nM. Controller 3 corresponds to an increase in RBS strength (i.e., a decrease in $k_{L_f} = 10^4$ nM). Controller 4 corresponds to a *tetR*-based implementation which changes the following parameters $k_{X_r} = 350$ nM, $\mu_f = 5.6$ nM and $\eta_f = 2$.

This is a modified and improved version of the μ-lower bound algorithm originally developed in [9], which did not exploit the use of the LFT-free formulation. Specifically,

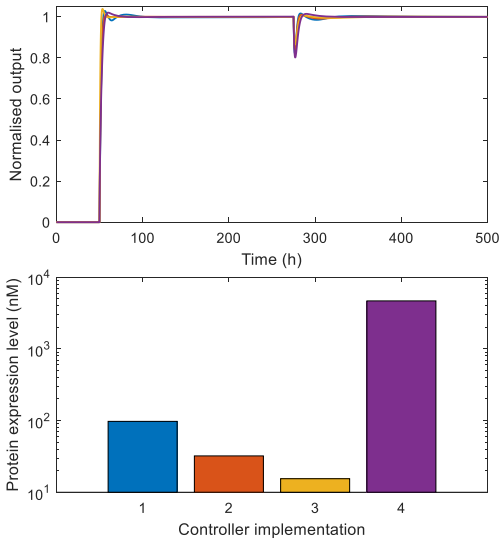

Fig. 7. Simulations of the different biological implementations of the controller using the non-linear model. Levels of p_1 normalised by final protein concentration are shown. Inputs: $u_1 = u_2 = 0$ nM while $t < 50$ h. $t > 50$ h, $u_1 = 500$ nM. $t > 275$ h, $u_2 = 500$ nM. *Upper*, dynamics normalised by final steady state output. *Lower*, steady state expression level.

here the expansion step (shown in Figure 5) is improved. Previously, this involved moving the centre of the box to the δ whose sign combination was found last, whereas in the current algorithm the centre of the box is placed in the middle between two δ's whose sign combinations were found last and second last. This avoids occasional problems with the algorithm switching between two regions for many iterations, and significantly improves its convergence properties.

IV. μ-Analysis of the Translational Controller

We use the above procedure to quantify and compare the stability robustness of four different potential biological implementations of the controller which act to modify key controller design parameters. We analyse three controllers based on the tightly binding LacI repressor, with varying p_f gene copy numbers and RBS strength, and one based on the TetR repressor (Figure 6) which changes dissociation constants and level of cooperativity. We set the uncertainty level for all 36 circuit and controller parameters at $\pm 40\%$ of their nominal values. As shown in Figure 6, our analysis indicates that all potential controller implementations are guaranteed to be stable for this level of uncertainty, since both μ-bounds are less than 1 at all frequencies. Total computing time to calculate the bounds for each controller was approx. 1 hour (with frequencies calculated in parallel on a 4 core Intel i7 processor with 32 GB RAM). Increasing $g_{f,T}$ (the copy number of the p_f gene) increases robustness, with the upper bound falling from 0.85 to 0.76. Decreasing k_{L_f} (i.e., increasing the strength of the p_f ribosome binding site) also increases robustness in comparison to the original case. Changing the repressor used to implement the controller from LacI to another common repressor TetR (hence changing its dissociation constant and co-operativity) also increases the robustness of the controller, (maximum μ-upper bound of 0.76).

Figure 7 (*upper*) confirms that the improvements in robustness offered by the different implementations do not come at the expense of dynamic performance. However, in addition to response times, steady-state protein concentrations are another important performance metric for many biotechnological applications, since different concentrations of the final protein can result in different noise profiles, growth effects, or rates of downstream chemical reactions (if the protein is an enzyme). Figure 7 (*lower*) shows that, in addition to its strong robustness properties, the tetR-based controller has significantly higher steady-state protein output than the lacI-based controllers, making it an attractive candidate for experimental implementation.

V. Conclusion

In this letter, we have considered the problem of formally quantifying the robustness of resource allocation controllers to parametric uncertainty using μ-analysis. Detailed modelling of resource sharing mechanisms in the closed-loop system revealed that the effects of uncertainty cannot be represented in the form of an LFT, as required by standard μ-analysis tools. We therefore applied an alternative approach, based on a geometric formulation of the μ-analysis problem, that allows the computation of tight bounds on μ without the need to represent the uncertain closed-loop system in the form of an LFT. This allowed us to evaluate and compare the robustness of alternative potential biological implementations of the controller, thus providing useful guidelines for the construction of robust resource allocation circuitry for multiple future biotechnological applications. The proposed approach should be applicable for analysing the robustness of many kinds of future synthetic biological control circuits.

References

[1] Y. Qian, H.-H. Huang, J. I. Jiménez, and D. Del Vecchio, "Resource competition shapes the response of genetic circuits," *ACS Synth. Biol.*, vol. 6, no. 7, pp. 1263–1272, 2017.

[2] F. Ceroni, R. Algar, G.-B. Stan, and T. Ellis, "Quantifying cellular capacity identifies gene expression designs with reduced burden," *Nat. Methods*, vol. 12, no. 5, pp. 415–423, 2015.

[3] A. Gyorgy *et al.*, "Isocost lines describe the cellular economy of genetic circuits," *Biophys. J.*, vol. 109, no. 3, pp. 639–646, 2015.

[4] M. Scott, C. W. Gunderson, E. M. Mateescu, Z. Zhang, and T. Hwa, "Interdependence of cell growth and gene expression: Origins and consequences," *Science*, vol. 330, no. 6007, pp. 1099–1102, 2010.

[5] A. P. S. Darlington, J. Kim, J. I. Jiménez, and D. G. Bates, "Dynamic allocation of orthogonal ribosomes facilitates uncoupling of co-expressed genes," *Nat. Commun.*, vol. 9, no. 1, p. 695, 2018.

[6] O. Rackham and J. W. Chin, "A network of orthogonal ribosome·mRNA pairs," *Nat. Chem. Biol.*, vol. 1, no. 3, pp. 159–166, 2005.

[7] A. P. S. Darlington, J. Kim, J. I. Jimenez, and D. Bates, "Engineering translational resource allocation controllers: Mechanistic models, design guidelines, and potential biological implementations," *Bioxriv Pre-Print*, doi: 10.1101/248948.

[8] S. Cardinale and A. P. Arkin, "Contextualizing context for synthetic biology–identifying causes of failure of synthetic biological systems," *Biotechnol. J.*, vol. 7, no. 7, pp. 856–866, 2012.

[9] J. Kim, D. G. Bates, and I. Postlethwaite, "A geometrical formulation of the μ-lower bound problem," *IET Control Theory Appl.*, vol. 3, no. 4, pp. 465–472, Apr. 2009.

[10] Y.-B. Zhao, J. Kim, and D. G. Bates, "LFT-free μ-analysis of LTI/LPTV systems," in *Proc. IEEE Int. Symp. Comput.-Aided Control Syst. Design*, Denver, CO, USA, 2011, pp. 638–643.